Transportation of single cell and microbubbles by phase-shift introduced to standing leaky surface acoustic waves

Long Meng,[1,a)] Feiyan Cai,[1,a)] Zidong Zhang,[1] Lili Niu,[1] Qiaofeng Jin,[1] Fei Yan,[1] Junru Wu,[2] Zhanhui Wang,[1] and Hairong Zheng[1,b)]
[1]*Paul C. Lauterbur Research Center for Biomedical Imaging, Institute of Biomedical and Health Engineering, Shenzhen Institutes of Advanced Technology, Chinese Academy of Sciences, Guangdong 518055, China*
[2]*Department of Physics, University of Vermont, Burlington, Vermont 05405, USA*

(Received 11 August 2011; accepted 27 September 2011; published online 20 October 2011)

A microfluidic device was developed to precisely transport a single cell or multiple microbubbles by introducing phase-shifts to a standing leaky surface acoustic wave (SLSAW). The device consists of a polydimethyl-siloxane (PDMS) microchannel and two phase-tunable interdigital transducers (IDTs) for the generation of the relative phase for the pair of surface acoustic waves (SAW) propagating along the opposite directions forming a standing wave. When the SAW contacts the fluid medium inside the microchannel, some of SAW energy is coupled to the fluid and the SAW becomes the leaky surface wave. By modulating the relative phase between two IDTs, the positions of pressure nodes of the SLSAW in the microchannel change linearly resulting in the transportation of a single cell or microbubbles. The results also reveal that there is a good linear relationship between the relative phase and the displacement of a single cell or microbubbles. Furthermore, the single cell and the microbubbles can be transported over a predetermined distance continuously until they reach the targeted locations. This technique has its distinct advantages, such as precise position-manipulation, simple to implement, miniature size, and noninvasive character, which may provide an effective method for the position-manipulation of a single cell and microbubbles in many biological and biomedical applications. [doi:10.1063/1.3652872]

I. INTRODUCTION

Precise transportation of a single cell is crucial in various areas of biomedical research, including molecular biology,[1,2] biochemistry,[3,4] and biophysics.[5,6] The ability to move cells precisely to a desired location would make it easier to transfect a single cell, change its gene expression, investigate its heterogeneity, and study the interaction between individual cells. The manipulation of single cell presents a variety of challenges. The critical requirement for the single cell manipulation technique is its accuracy and reproducibility to transport the cell to a targeted location. Meanwhile, cells must be handled gently and their viability has to be maintained; any mechanical perturbation to their biochemical pathways and molecular integrity has to be minimized.

To date, a variety of approaches have been adopted to transport cells in a microfluidic device.[7–12] For instance, optoelectronic tweezers provide a high-resolution in transporting cells, but they require intricate optical setup, which is difficult to be integrated with a microfluidic device.[7] Electrokinetic pumping is widely used in controlling fluid flow in microfluidic devices, and thus may serve as an alternative solution to transport the cells. However, the high electric

[a)]L. Meng and F. Y. Cai contributed equally to this work.
[b)]Electronic mail: hr.zheng@siat.ac.cn.

field may induce heating, which may cause strong adverse effects on cell viability, especially when dealing with the mammalian cells.[13] Techniques based on magnetic fields allow low power consumption to transport cells, but the attachment of magnetic beads to cells is the prerequisite for such methods which involve sophisticated techniques.[14] Accordingly, there is needed to develop other new methods for single cell position manipulation which should meet multiple requirements: precise, easy to implement, and noninvasive.

The usage of acoustical method as a non-contact cell manipulation technique has generated great interest.[15–20] The acoustic method can handle bioparticles regardless of their surface chemistry or charge properties, which may provide a potentially promising approach to manipulate a single cell. Available methods for controlling the transportation of bioparticles based on bulk waves are realized mainly by switching/changing the relative phase,[21] resonant mode,[22] and actuation frequency.[23] However, the manipulation of nanoscale particles usually requires high frequency of waves for the wavelength need to be comparable to the size of the particle and the attenuation of the bulk acoustic wave in liquid is proportional to square of frequency[24]. Part of the loss becomes temperature rise of the medium and the associated thermal conduction irreversibly while part of it may be converted to streaming of the medium. The energy loss particularly of the former reduces the amount of acoustic energy converted to the kinetic energy of the particles inside the microchannel and makes the system less suitable to operate at a higher frequency as required for the manipulation of nanoparticles. In addition, difficulties in miniaturization and integration of the bulk wave device based on piezoelectric ceramics (PZT) have limited the potential applications of emerging microfluidic systems.

Recently, surface acoustic wave (SAW) based microfluidics have been proven to be more suitable for a variety of biomedical applications,[25–32] because its localization of the energy near the substrate surface leads to high energy density along the surface, the great design flexibility of the transducer is readily operated at a high frequency, and the utilization of micro-electronic-mechanical system (MEMS) technology has the advantage in miniaturization and integration. Li *et al*. demonstrated the concentration of cells suspended within a droplet by acoustic streaming.[33] Franke *et al*. showed a rapid cell-sorting scheme, directing the cells in a continuous flow at high sorting rates.[34] However, applications of acoustic streaming to manipulate cells have been shown that it is difficult to transport cells over a predetermined distance and position them to a precise location. Shi *et al*. used acoustic radiation force to retain the cells at the pressure nodes in a standing SAW (SSAW) field.[35] Nevertheless, the acoustic pressure nodes or antinodes inside the microchannel are stationary, which fails to transport cells to desired positions.

In this paper, we present a microfluidic device that can provide a precise and simple means to transport an individual cell and multiple microbubbles. The basic principle is based on introducing a phase-shift to standing leaky surface acoustic wave (SLSAW). The position of the pressure nodes varies linearly with the phase difference of the electric voltages applied to two identical interdigital transducers (IDTs). Furthermore, the experimental results show that both cells at the individual-level and microbubbles at the group-level could be transported over a predetermined distance continuously and reach desired targets.

II. METHODS AND MATERIAL

A. Working mechanism

The mechanism of transportation of cells based on phase-shift with SLSAW is illustrated in Fig. 1. The microfluidic device consists of a polydimethyl-siloxane (PDMS) microchannel located symmetrically between two identical IDTs which form a pair of SAW generators. When applied the same electrical signal to the two IDTs, the piezoelectric substrate begins to vibrate, and SAW can be generated. As shown in Fig. 1(a), when the SAW reaches the microchannel filled with a liquid (water), mode conversion takes place; Rayleigh waves will be converted to the leaky SAW (LSAW) along the surface and two beams of bulk acoustic (longitudinal) waves (BAW) in the fluid. After mode conversion, part of energy of the SAW will convert to BAW, and the rest of acoustic energy lies in the LSAW. The BAW propagates along

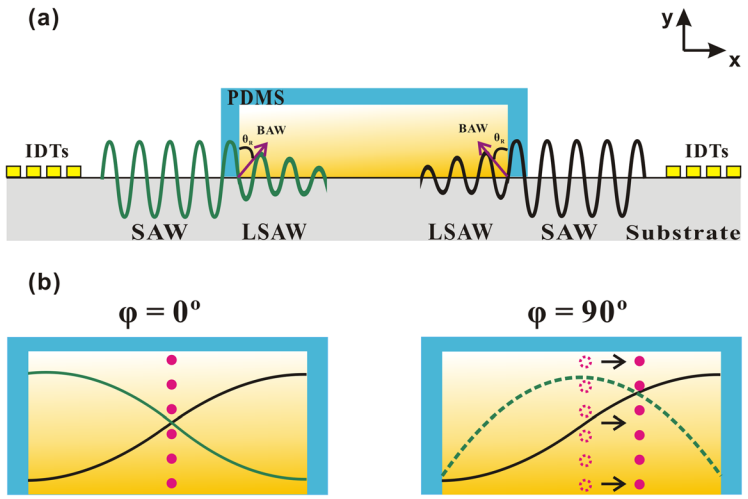

FIG. 1. (a) Schematic of the interaction of the Rayleigh wave with the fluid medium. (b) Schematic of the transportation of cells by introducing the phase-shift to a standing wave. Varying the relative phase between the input signals, the pressure nodes translate correspondingly, leading to the transportation of the cells.

the Rayleigh angle $\theta_R = \sin^{-1}(c_w/c_s) = \sin^{-1}(1490/3900) = 22.5^\circ$ in the liquid. When the height of microchannel is much smaller than the wavelength of SAW, most energy of the SAW still lies in the form of LSAW.[36] The displacement of LSAW decays exponentially along the positive y direction in the liquid medium, and the energy of the LSAW is confined along the x axis direction. Due to the velocity of the SAW and LSAW are near equal, the wavelength of the LSAW is approximately equal to that of the SAW at the same excitation frequency. The superposition of the two LSAW travelling in opposite directions along the x axis generates a standing wave. As a simple mathematical model by neglecting the damping, the acoustic pressure of the standing wave may be expressed by

$$\begin{aligned} P &= P_0 \cos(\omega t - kx + \varphi) + P_0 \cos(\omega t + kx) \\ &= 2P_0 \cos(\omega t + \varphi/2) \cos(kx - \varphi/2), \end{aligned} \tag{1}$$

where P_0, k, ω correspond to pressure amplitude, wave number, angular frequency of the LSAW and φ is the relative phase between the LSAW.

The particles suspended in fluid experienced the acoustic radiation force in the standing wave can be described as[37]

$$F = -\left(\frac{\pi p_0^2 V_c \beta_w}{2\lambda}\right) \Phi(\beta, \rho) \sin(2kd), \tag{2}$$

$$\Phi(\beta, \rho) = \frac{5\rho_c - 2\rho_w}{2\rho_c + \rho_w} - \frac{\beta_c}{\beta_w}. \tag{3}$$

Here, $\Phi(\beta, \rho)$ describes the relationship of density and compressibility between the particle and the medium, which plays a role in determining the direction of the radiation force. If $\Phi(\beta, \rho) > 0$, the particle will be forced to the pressure nodes; otherwise, it will be moved to the pressure antinodes. Here, λ, V_c are the wavelength, and the volume of the particle, respectively; the densities of the particle and the medium are denoted by ρ_c and ρ_w, and the corresponding compressibility β_c and β_w, respectively, d is the distance between the particle and the nearest pressure nodes.

In one-dimensional SLSAW, the cells assemble at the pressure nodes resulting in a pattern of series of lines for $\Phi(\beta, \rho) > 0$. Varying the relative phase between the excitation voltages,

the position of the pressure nodes of the SLSAW can be translated correspondingly [Fig. 1(b)]. The relationship between the linear translation Δx of the pressure nodes and relative phase φ can be given by

$$\Delta x = \frac{1}{2k}\varphi = \frac{\lambda}{720^\circ}\varphi \quad \varphi \in [0^\circ, 360^\circ]. \tag{4}$$

This expression indicates that the position of the pressure nodes in x-direction varies linearly with the φ. The pressure nodes can be transported with the distance of half a wavelength when φ changes from 0° to 360°. When φ changes from 0° to 180°, the places where originally are pressure antinodes become nodes and the pressure nodes become antinodes again as the change of φ from 180° to 360°.

B. SAW-PDMS microfluidic device

The single cell manipulation device is a bonded device including a PDMS microchannel, a pair of SAW generators, and a printed circuit board (PCB), as shown in Fig. 2. The PDMS microchannel was fabricated by standard photolithography procedures. The microchannel had a width of 200 μm and a height of 50 μm. The SAW generator was fabricated by deposition of aluminium layer (200 nm thick) on a 128° Y-rotated, X-propagating $LiNbO_3$ substrate (1 mm thick). The electrode spacing was 100 μm, generating a SAW with a wavelength of 200 μm at a resonance frequency of 19.8 MHz. Both edges of substrate were coated with sound absorber material (synthetic resin) to reduce the interface reflections. The PCB, with a rectangular-shaped hole in the centre, was glued to the SAW generator by sound absorber material for supplying the input power. Oxygen plasma treatment for both PDMS microchannel and substrate surface activation was carried out at a flow rate of 50 sccm and a power of 150 W. Then, the PDMS microchannel was precisely mounted on the alignment markers of the substrate to ensure the microchannel was perpendicular to the acoustic propagation. A post-bake process at 80 °C for 30 min was conducted to improve the bonding strength.

C. Sample preparation

To demonstrate the transportation performance of the microfluidic device at the group-level and individual-level, respectively, the microbubbles and the single human breast cancer cell were used in the experiments. The microbubbles composed of octafluoropropane (C_3F_8) gas encapsulated by a phospholipid shell were in-house fabricated by the mechanical agitation method.[38] The mean diameter of the microbubbles was 0.87 μm with a standard deviation of 0.53 μm, and 78.38% microbubbles had diameters less than 1 μm measured by the particle size analyzer (AccuSizer 780, Particle Sizing Systems, Santa Barbara, CA). The cells (human breast cancer cell lines MDA-MB-453) were purchased from Shanghai Institutes for Biological Sciences, Chinese Academy of Sciences. Both the microbubbles and cells were labeled using the lipid-binding fluorescent carbocyanine dyes DiI (Sigma-Aldrich). Cell viability was assessed by

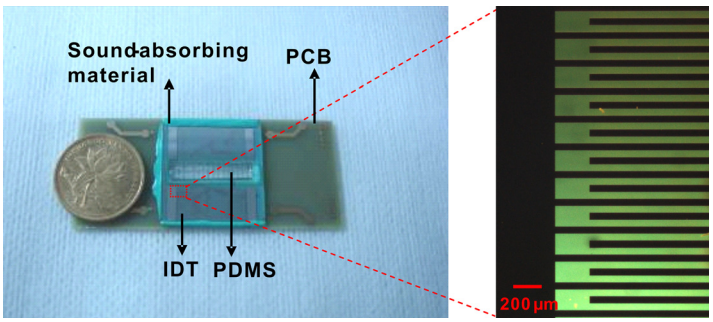

FIG. 2. Photograph of the microfluidic device. Inset: The finger pairs of the IDT on the substrate.

calcein acetoxymethyl ester (Calcein AM) and propidium iodide (PI) uptake. Calcein AM is taken up and cleaved by esterases present within living cells, yielding green fluorescence, whereas PI is only taken up by dead cells, which become red fluorescent.

D. Experimental system

The performance of the bonded device was recorded by a CCD camera mounted on a fluorescence microscope (Eclipse 50i, Nikon, Japan). Two independent continuous sinusoidal signals were generated by a dual-channel arbitrary signal generator (AFG3102, Tektronix, USA) without any amplifiers, transmitted by two identical signal cables, and then applied to both IDTs separately. The applied voltage to each IDT in all experiments was held constant at peak-to-peak amplitude of 10 V providing a driving power of 60 mW measured by a signal analyzer (FSQ40, Rohde & Schwarz, Germany). The microbubbles and cells were driven into the microchannel by a syringe pump (Top-5300, Top Syringe Pump, Japan).

III. RESULTS AND DISCUSSIONS

A. Manipulation of microbubbles

To investigate the performance of the device at the group-level, a large number of microbubbles (6.8×10^8 bubbles/ml) with red fluorescence were injected into the microchannel at a flow rate of 5 μl/min. The microbubbles moved rapidly along the z direction by the pressure driven flow, as shown in Fig. 3(a). When both IDTs were excited by two identical input signals, the microbubbles began to aggregate immediately [Fig. 3(b)]. After about 10 s, the microbubbles were aligned in a straight line and the fluorescence intensity increased as the number of the aligned microbubbles increases [Figs. 3(c)–3(d)]. When the φ was set to 100°, the microbubbles moved to the negative direction along the x axis for some distance [Fig. 3(e)]. Then, by continuous adjusting the φ to 200°, the microbubbles kept on moving towards the bottom wall of the microchannel for the same increment of distance [Fig. 3(f)]. In contrast, decreasing the φ to 100°, the microbubbles moved in an opposite direction [Fig. 3(g)], and the microbubbles could return back to the initial position by further decreasing φ to 0° [Fig. 3(h)]. A real-time video showing the transportation of the microbubbles is provided (see Fig. 3).

As shown in Fig. 3, the microbubbles move almost the same distance at every variation of the phase-shift $\Delta\varphi$ of 100°. To quantitatively evaluate the displacement of microbubbles, IMAGEJ software (NIH, Bethesda, MD) was used to measure the transportation distance based on optical image sequences. The average transportation distance of each time is 25.8 ± 1.41 μm, which agrees well with the theoretical value (27.8 μm). Moreover, if $\Delta\varphi > 0$,

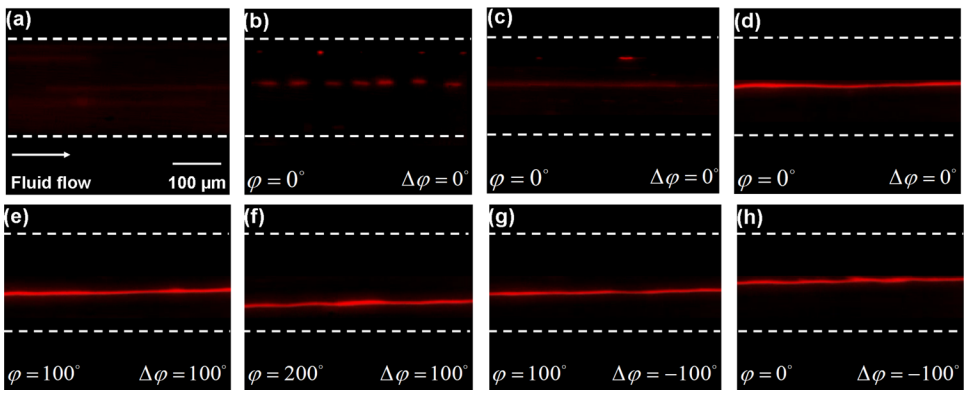

FIG. 3. A movie illustrating the continuous transportation of microbubbles (red fluorescence) under input power = 60 mW actuation at a flow rate of 5 μl/min. The alignment of the microbubbles was observed in x-z plane of the microchannel (a-d). The alignment position of microbubbles was varied by changing the relative phase (e) $\varphi = 100°$, (f) $\varphi = 200°$, (g) $\varphi = 100°$, (h) $\varphi = 0°$ (enhanced online) [URL: http://dx.doi.org/10.1063/1.3652872.1].

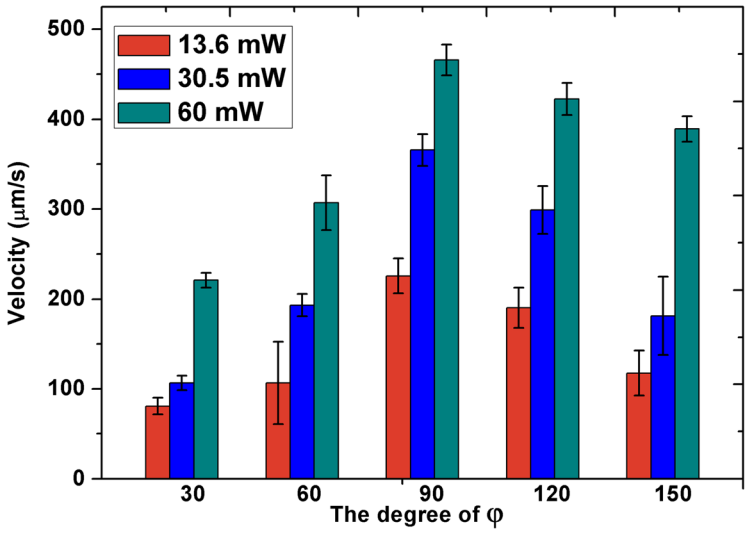

FIG. 4. The transportation velocity of the microbubbles verse relative phase at various input power. The microbubbles were transported from the location where $\varphi = 0°$ to the place where $\varphi = 30°$, 60°, 90°, 120°, and 150°, respectively.

the microbubbles moved along the negative x-axis direction; while $\Delta\varphi < 0$, the microbubbles moved towards the positive x direction. Thus, the displacement and the movement direction are entirely dependent on the φ and $\Delta\varphi$. For a constant φ, the position of the microbubbles is almost the same, which ensures a favourable reproducibility.

The acoustic radiation force on the microbubbles changes sinusoidally with the distance between the microbubbles and the pressure nodes.[39] Once the position of the pressure nodes changes by introducing a phase shift, the acoustic radiation force that the microbubbles experienced varies correspondingly, which is the reason for generating a translational motion. As shown in Fig. 4, the transportation velocity increases with the change of φ from 30° to 90° and then decreases when φ changes from 90° to 150°; the maximum average velocity can be attained by adjusting the φ to 90°, which shows the relationship between the transportation velocity versus relative phase is similar to that between the acoustic radiation force versus relative phase. In addition, the magnitude of acoustic radiation force is proportional to the input power.[40] It is possible to investigate the relation between the input power and the velocity to reveal the relation between the acoustic radiation force and the velocity. Fig. 4 shows the transportation velocity increases with the increase of the input power. The maximum average velocity of the transportation is approximately 465 μm/s, which means it would take less than 0.1 s to translate the distance of one-quarter wavelength. It is observed that the response time of the realignment is almost instantaneous, which seemed to enable the real-time dynamics of manipulation.

B. Manipulation of single cell

The human breast cancer cell of MDA-MB-453, a typical model of cancer cells, was selected to characterize the transportation performance of the device at the individual-level. An almost spherical shape of single MDA-MB-453 cell with a diameter of about 10 μm was infused into the microchannel (dashed lines). When there was no phase shift, the cell was retained to the pressure node in the centre of the microchannel, as shown in Fig. 5(a). Setting the value of φ to $-100°$, the cell moved towards the positive direction of x-axis for a distance of 27.6 μm [Fig. 5(b)]. While adjusting the value of φ to $-150°$, the cell kept on moving in the positive x direction, but the distance of transportation was reduced to a half value correspondingly, about 13.9 μm [Fig. 5(c)]. Then, making φ to $-50°$, the cell moved toward a position closer to the initial position [Fig. 5(d)]. Finally, the φ was further reduced to 0°, the cell went on moving in the negative x direction and returned back to the location where it started

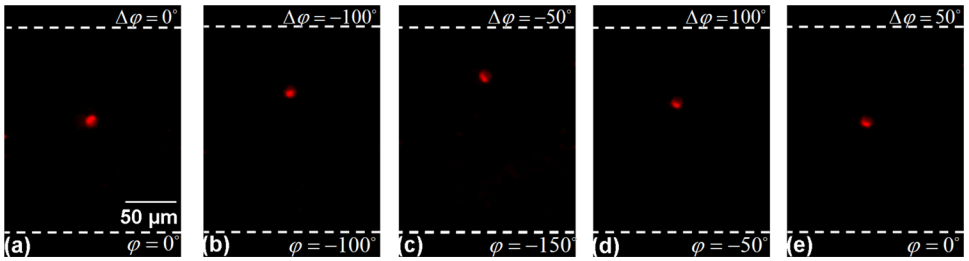

FIG. 5. A movie illustrating the continuous transporting the single cell (red fluorescence) in the microchannel (dashed lines) under input power = 60 mW actuation by varying the relative phase of (a) 0°, (b) −100°, (c) −150°, (d) −50°, and (e) 0°. The displacement of the single cell in (c)and (e) is half of the displacement in (b) and (d). Through a series of manipulation, the single cell can return back to the initial position (enhanced online) [URL: http://dx.doi.org/10.1063/1.3652872.2].

[Fig. 5(e)]. A real-time video showing the transportation of the single cell is provided (see Fig. 5).

Further experiments were carried out to investigate the displacement of the single cell as a function of φ. Fig. 6 shows the experimental data of the average displacement in the x-direction at various φ, and the red line represents the fitting curve of the experimental points. It can be seen that there is a fairly good linear relationship between the displacement and the relative phase, which agrees well with the results predicted in Eq. (4).

It is known that ultrasound has thermal and mechanical effects and many studies have shown that the ultrasound wave with low acoustic pressure will not influence the viability of the cell, even in long-term manipulation.[41,42] The thermal effect is induced by absorption of the mechanical oscillation, which may potentially influence the cell viability in the microchannel. To investigate the change of the temperature of the device, an infrared thermometer was used to measure the temperature profile in the volume of the microchannel. Fig. 7 shows the temperature profile as a function of the stimulus duration when the input power is held constant at 60 mW. The longest stimulus duration in this study is less than 1 min and the temperature of the device increases from 18.5 °C to 19.2 °C, which should have negligible adverse biological effects on cells.

To further verify the noninvasive character of this technique, the Calcein AM/PI double-staining was performed for quantitative analysis of the cell viability. Viable cells would exhibit green fluorescence due to the conversion of Calcein AM to calcein by intracellular esterases.

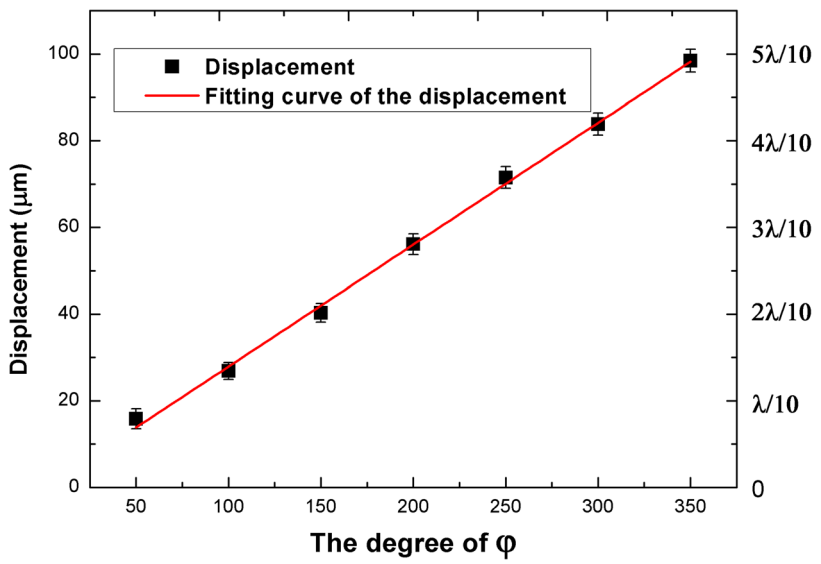

FIG. 6. Experimental data of the displacement at various φ and the fitting curve of the displacement (red line).

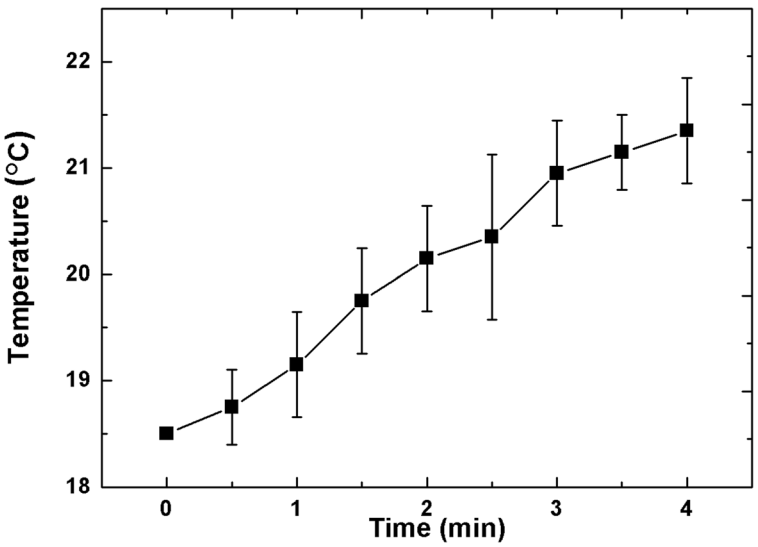

FIG. 7. The surface temperature of the device varies as a function of time. The RF power was held constant at 60 mW.

On the other hand, dead cell would emit red fluorescence since PI binds to double-stranded DNA by passing through disordered areas of dead cell membrane. The solution of cells was divided into three groups. The first group of the cells was kept incubated further at 37° carbon dioxide incubator (positive control). The second group of cells was infused into the

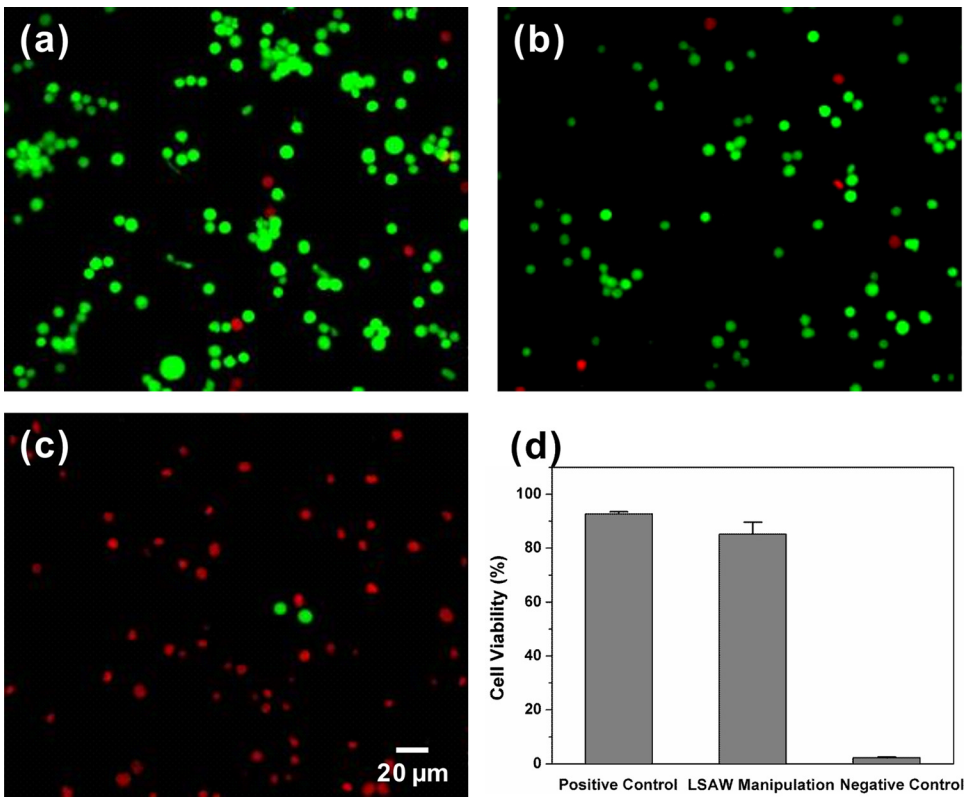

FIG. 8. Calcein AM/PI double staining assay to measure the cell viability. (a) Cells further cultured in the carbon dioxide incubator (Positive Control); (b) Cells manipulated by phase-shift SLSAW for 2 min; (c) Cells heated at 65°C for 1 h (Negative Control); (d) Quantitative analysis of the cell viability in each group.

microchannel, manipulated by acoustic radiation force (2 min), and then collected at the output channel. The cells in the third group were incubated at 65° for 1 h (negative control). Fig. 8 shows the fluorescence image and the viability of the cells at different groups. In the first group, almost entirely of cells exhibit green fluorescence and only a few cells emit red fluorescence [Fig. 8(a)]. A few dead cells may be attributed to the dissociation treatment with a trypsin-EDTA solution. Fig. 8(b) shows the state of cells after acoustic manipulation. The bright green fluorescence of the cells after manipulation does not differ significantly compared with Fig. 8(a). As shown in Fig. 8(d), about 85% the cells maintain their viability after manipulation for 2 min at an applied power of 60 mW, suggesting that the acoustic manipulation does not affect the viability of the cell. However, nearly all the cells in the third group emitted red fluorescence since 98% the cells were dead [Figs. 8(c)–8(d)]. These results confirm that the acoustic manipulation based on phase-shift SLSAW is a noninvasive or minimum-invasive method.

IV. CONCLUSIONS

This paper demonstrates both the individual cell and multiple microbubbles can be transported by the linear translation of pressure nodes of the SLSAW, generated by the shift of relative phase between voltages applied to two IDTs. By varying the relative phase, the single cell and microbubbles could be transported precisely to the target location in the microchannel. We have shown that there is a fairly good linear relationship between the displacement and the phase difference between the electric voltages applied to the two IDTs. Furthermore, this phase-shift device based on SLSAW is fabricated through the standard MEMS processes, facilitating miniaturization and mass production at considerably lower costs. We strongly believe that in the near future, the SAW based microsystems could be widely applied as general multipurpose tools for a variety of cell analysis tasks.

ACKNOWLEDGMENTS

The work was supported by National Basic Research Program 973 (Grant Nos. 2010CB732600, 2010CB534914, and 2011CB707903) from Ministry of Science and Technology, China, National Science Foundation Grants (Grant Nos. 81027006, 61020106008, 10904094, 11002152, 10904095, and 61002001).

[1]K. Schutze and G. Lahr, Nat. Biotechnol. **16**(8), 737 (1998).
[2]E. R. Kandel, Science **294**(5544), 1030 (2001).
[3]M. Lakso, J. G. Pichel, J. R. Gorman, B. Sauer, Y. Okamoto, E. Lee, F. W. Alt, and H. Westphal, Proc. Natl. Acad. Sci. U.S.A. **93**(12), 5860 (1996).
[4]C. Yi, C.W. Li, S. Ji, and M. Yang, Anal. Chim. Acta **560**(1–2), 1 (2006).
[5]J. Gimsa, T. Mller, T. Schnelle, and G. Fuhr, Biophys. J. **71**(1), 495 (1996).
[6]A. D. Mehta, M. Rief, J. A. Spudich, D. A. Smith, and R. M. Simmons, Science **283**(5408), 1689 (1999).
[7]P. Y. Chiou, A. T. Ohta, and M. C. Wu, Nature (London) **436**(7049), 370 (2005).
[8]E. W. H. Jager, O. Inganas, and I. Lundstrom, Science **28 8**(5475), 2335 (2000).
[9]B. R. Lutz, J.Chen, and D. T. Schwartz, Anal. Chem. **78**(15), 5429 (2006).
[10]M. Karle, J. Miwa, G. Czilwik, V. Auwarter, G. Roth, R. Zengerle, and F. von Stetten, Lab Chip **10**(23), 3284 (2010).
[11]Z. Wang, M. C. Kim, M. Marquez, and T. Thorsen, Lab Chip **7**(6), 740 (2007).
[12]T. Thorsen, S. J. Maerkl, and S. R. Quake, Science **298**(5593), 580 (2002).
[13]J. Voldman, Annu. Rev. Biomed. Eng. **8**(1), 425 (2006).
[14]Q. A. Pankhurst, J. Connolly, S. K. Jones, and J. Dobson, J. Phys. D: Appl. Phys. **36**(13), R167 (2003).
[15]J. Wu, J. Acoust. Soc. Am. **89** (5), 2140 (1991).
[16]T. Laurell, F. Petersson, and A. Nilsson, Chem. Soc. Rev. **36**(3), 492 (2007).
[17]O. Manneberg, B. Vanherberghen, J. Svennebring, H. M. Hertz, B. Önfelt, and M. Wiklund, Appl. Phys. Lett. **93**(6), 063901 (2008).
[18]S. Oberti, A. Neild, and J. Dual, J. Acoust. Soc. Am. **121**(2), 778 (2007).
[19]J. Lee, S. Y. Teh, A. Lee, H. H. Kim, C. Lee, and K. K. Shung, Appl. Phys. Lett. **95**(7), 073701 (2009).
[20]J. Jeong, J. Lee, C. Lee, S. Teh, A. Lee, and K. Shung, Biomed. Microdevices 13 (4), 779 (2011).
[21]C. R. P. Courtney, C. K. Ong, B. W. Drinkwater, P. D. Wilcox, C. Demore, S. Cochran, P. Glynne-Jones, and M. Hill, J. Acoust. Soc. Am. **128**(4), E195 (2010).
[22]P. Glynne-Jones, R. J. Boltryk, N. R. Harris, A. W. J. Cranny, and M. Hill, Ultrasonics **50**(1), 68 (2010).
[23]O. Manneberg, B. Vanherberghen, B. nfelt, and M. Wiklund, Lab Chip **9**(6), 833 (2009).
[24]L. E. Kinsler, A. R. Frey, A. B. Coppens, and J. V. Sanders, *Fundamentals of Acoustics*, 4th ed. (Wiley, New York, 1999).
[25]L. Y. Yeo and J. R. Friend, Biomicrofluidics **3**(1), 012002 (2009).

[26]J. Friend and L. Yeo, Rev. Mod. Phys. **83**(2), 647 (2011).
[27]H. Li, J. R. Friend, and L. Y. Yeo, Phys. Rev. Lett. **101**(8), 84502 (2008).
[28]L. Y. Yeo, H.-C. Chang, P. P. Y. Chan, and J. R. Friend, Small **7**(1), 12 (2011).
[29]A. Wixforth, C. Strobl, C. Gauer, A. Toegl, J. Scriba, and Z. v. Guttenberg, Anal. Bioanal. Chem. **379**(7), 982 (2004).
[30]J. Neumann, M. Hennig, A. Wixforth, S. Manus, J. O. Radler, and M. F. Schneider, Nano Lett. **10**(8), 2903 (2010).
[31]J. Shi, X. Mao, D. Ahmed, A. Colletti, and T. J. Huang, Lab Chip **8**(2), 221 (2008).
[32]Y. Jun Liu, X. Ding, Sz.-C. Steven Lin, J. Shi, I. Kao Chiang, and T. Jun Huang, Adv. Mater. **23**(14), 1575 (2011).
[33]H. Li, J. R. Friend, and L. Y. Yeo, Biomed. Microdevices **9**(5), 647 (2007).
[34]T. Franke, A. R. Abate, D. A. Weitz, and A. Wixforth, Lab Chip **9**(18), 2625 (2009).
[35]J. Shi, D. Ahmed, X. Mao, S. C. S. Lin, A. Lawit, and T. J. Huang, Lab Chip **9**(20), 2890 (2009).
[36]L. Meng, F. Y. Cai, Q. F. Jin, L. L. Niu, C. X. Jiang, Z. H. Wang, J. R. Wu, and H. R. Zheng, Sens. Actuators B (unpublished).
[37]K. Yosioka and Y. Kawasima, Acustica **5**(3), 167 (1955).
[38]K. W. Ferrara, M. A. Borden, and H. Zhang, Accounts Chem. Res. **42**(7), 881 (2009).
[39]A. A. Doinikov, Recent Res. Devel. Acoustics **1**, 39 (2003).
[40]A. D. Pierce, Acoustics: An Introduction to its Physical Principles and Applications (Acoustical Society of America, New York, 1989).
[41]H. Li, J. Friend, L. Yeo, A. Dasvarma, and K. Traianedes, Biomicrofluidics **3**(3), 034102 (2009).
[42]J. Hultstrom, O. Manneberg, K. Dopf, H. M. Hertz, H. Brismar, and M. Wiklund, Ultrasound Med. Biol. **33**(1), 145 (2007).